Electronic energy-structure calculations for orthorhombic InI single crystals

1994 J. Phys.: Condens. Matter 6 183

(http://iopscience.iop.org/0953-8984/6/1/019)

J. Phys.: Condens. Matter 6 (1994) 183–202. Printed in the UK

Electronic energy-structure calculations for orthorhombic InI single crystals

M I Kolinko

Faculty of Physics, Lviv I Franko University, Wulycja Volodymyra Velykogo 97/72, Lviv, 290053, Ukraine

Received 8 April 1993, in final form 10 September 1993

Abstract. Electronic and ground-state properties of indium iodide in the orthorhombic TlI-type structure (space group D_{2h}^{17}) are reported. These properties are derived from the one-particle Kohn–Sham equations in the local-density approximation. The *ab initio* norm-conserving non-local pseudopotential of Bachelet, Hamann and Schlüter is used. The corresponding calculational technique is described briefly. Analytical expressions for the matrix elements are obtained. Results are presented for the valence and conduction band energies, densities of states, effective masses and charge densities. In terms of these, a consistent explanation of various experimental measurements of InI single crystals has been obtained. Furthermore, by examining the orbital character and the calculated charge densities of various states, the origin of the bonding in indium iodide has been determined.

1. Introduction

Among the group III monohalides, cubic thallous halides have been investigated more extensively, and a number of works have been examined by Kobayashi (1976). On the other hand, indium halides (InI, InBr, InCl) also belong to the III–VII compounds. They crystallize in the orthorhombic structure of TlI type (space group $CmCm$ (D_{2h}^{17})), which differs from that of the well investigated cubic thallous halides. The crystal structure of InI has been determined by Jones and Templeton (1955) and discussed by Levy and Mooser (1972), who, in addition, presented some preliminary results on optical and electrical measurements.

From the compounds with such structure, particular attention has been paid to TlI, from both the experimental (optical properties and phase transitions: Ohno *et al* 1986, 1987, Lowdes and Perry 1978, Van Dyke and Samara 1975; ultraviolet photoelectron spectroscopy (UPS): Porte and Maire 1980) and the theoretical (band-structure calculations: Van Dyke and Samara 1975, Kolinko *et al* 1992a; chemical bonding exploration: Otto *et al* 1992) points of view.

As for InI properties, they have not yet been studied so extensively: optical spectra of InI single crystals at low temperatures were investigated by several authors (Levy and Mooser 1972, Ohno *et al* 1978, 1980, 1985, Blonskii *et al* 1986, Jin *et al* 1989, Krochuk *et al* 1991, Yoshida *et al* 1984); the lattice dynamics response was examined by means of infrared (IR) and Raman spectroscopy (Clayman *et al* 1982); and indium halide (InI, InCl, InBr) valence band spectra were obtained by x-ray photoelectron spectroscopy (XPS) (Porte 1982); but no attempts have been made to perform energy band-structure calculations. InI experimental spectra show strong dichroism appropriate for the anisotropic crystal structure (Jin *et al* 1989, Krochuk *et al* 1991, Yoshida *et al* 1984). Especially, in the reflection spectra near the absorption edge, a sharp structure of exciton transitions is revealed at 4.2 K, which

0953-8984/94/010183+20$07.50

demonstrates strong anisotropy towards polarization directions (Ohno *et al* 1978). Owing to the lowest transition, the first exciton peak is located at 2.018 eV and is observed for *c*-polarized light. The $E\|a$ spectrum suggests that this transition is forbidden. It should be noted that the indirect exciton absorption edge was observed in InBr for $E\|c$ (Yoshida *et al* 1984), while in InI the presence of structure that depends on indirect absorption (Levy and Mooser 1972, Ohno *et al* 1978) has been denied in the following works (Yoshida *et al* 1984, Ohno *et al* 1980). Owing to free and bound excitons, strong edge emission has been observed (Ohno *et al* 1980), which led to the supposition of the direct nature of the minimum band gap in InI. The binding energy of the direct exciton appeared to be fairly small. It is estimated for InI to be 4.3 meV, assuming the hydrogenic model for the exciton series (Ohno *et al* 1978). Multiple longitudinal optic (LO) phonon scattering has been observed in InI (Ohno *et al* 1985) when excited above the first exciton energy. Moreover, scattering lines were characterized by an intensity alternation where even-numbered lines were stronger than odd-numbered ones. This phenomenon has been observed neither in II–VI nor in III–V compounds. The absorption coefficients calculated by Jin *et al* (1989) at the maxima of the exciton band for both $E\|c$ and $E\|a$ are at least one order of magnitude larger than those obtained by Blonskii *et al* (1986). While this compound is anisotropic, the IR results (Clayman *et al* 1982) appeared surprisingly to be independent of polarization. Several investigations of thallium iodide structural phase transition have been published (Lowdes and Perry 1978). Except for InCl, such a phase transition does not occur in indium halides. The existence of an improper ferroelastic phase with temperature hysteresis of phase transition near 5 K in the temperature region 4.2–25 K was found in indium iodide (Kityk *et al* 1992). Photostimulated changes in InI single crystals were discussed in the paper by Kolinko *et al* (1992b).

Notwithstanding intensive experimental efforts on pure InI and its solid solutions ($InBr_{1-x}I_x$ (Yoshida *et al* 1984); $In_xTl_{1-x}I$ (Blonskii *et al* 1992, Brodin *et al* 1992)), some more principal questions are left unsettled. In particular, the nature of interband absorption and chemical bonding (Otto *et al* 1992) of these compounds are under discussion now.

The band-structure calculation of orthorhombic TlI performed by Van Dyke and Samara (1975) has been used up to now for InI and other indium halide optical spectra identification. This calculation was performed in the process of study of the insulator–metal phase transition in TlI cubic modification in a simplified crystal model (overlapping atomic potentials) and, by today's standards, with the crude approximation for the exchange–correlation potential (Slater exchange coefficient $\alpha = 1$). Therefore, the calculation possessed only empirical character and the $\rho(r)$ charge-density distribution (and $E(k)$ dispersion as well) was approximate. However, the results for TlI single crystals (space group D_{2h}^{17}) are not completely true for these approaches in these compounds (Kolinko *et al* 1992a). A great number of energy optima with almost the same values for bands that form a forbidden gap were determined and weak band dispersion was noticed in the work that was carried out with a non-local norm-conserving pseudopotential. Besides, the hypothesis of the non-correct usage of the electron $E(k)$ spectrum of orthorhombic TlI for optical spectra identifiction of isostructural indium halides was proposed.

Therefore, the exchange–correlation interactions are of great interest for the energy spectrum of the compounds mentioned above. Charge-density distribution study appears to be of primary importance, as it promotes understanding of the nature of the chemical bond.

In principle, layered structures that crystallize in the D_{2h}^{17} lattice differ from conventional materials in their physical properties. Further, in this case, there has been no accumulation of experimental data that complements the parametrization in conventional empirical calculation of physical quantities. Thus, since there is no assurance that empirical approaches

with adjustable parameters provide us with reliable information, first principles calculations are required to investigate various properties of these single crystals.

In order to get precise information on band-structure parameters (including the k-space band dispersion) and evaluations of $\rho(r)$ charge density, *ab initio* self-consistent band-structure calculations of InI have been performed applying the non-local norm-conserving pseudopotential (Hamann *et al* 1979).

2. Calculation techniques

Hohenberg, Kohn and Sham (Hohenberg and Kohn 1964, Kohn and Sham 1965) have shown that the ground-state properties of an interacting electron system under an external field are determined by an effective one-electron equation containing an exchange–correlation potential in addition to the usual Hartree potential and the external one. In the local-density-functional formalism, the total energy is described by the functional

$$E[\rho] = T[\rho] + \int \mathrm{d}r\, V(r)\rho(r) + \frac{e^2}{2}\int \frac{\rho(r)\rho(r')}{|r-r'|}\,\mathrm{d}r\,\mathrm{d}r' + E_{\mathrm{xc}}[\rho] \qquad (1)$$

which is a sum of items that are all functionals of the total charge density $\rho(r)$. The first term in (1) corresponds to the kinetic energy of the non-interacting electronic system, the second to the potential energy of electrons in the crystal potential, the third to the electrostatic part or Hartree energy and the last to the exchange–correlation energy.

According to Kohn and Sham (1965), a variational solution of equation (1) can be obtained by self-consistently solving a set of Schrödinger-type equations:

$$\left(-\tfrac{1}{2}\nabla^2 + V_i(r) + \int \frac{\rho(r)}{|r-r'|}\,\mathrm{d}r + \mu_{\mathrm{xc}}(\rho)\right)\psi_{nk} = E_{nk}\psi_{nk} \qquad (2)$$

where μ_{xc} is the exchange–correlation potential of a chemically homogeneous interacting gas and E_{nk} are the Lagrange factors that form the spectrum of one-particle energy states. The Hamiltonian eigenvector functions take the form $\psi_{nk} = \exp(\mathrm{i}\boldsymbol{k}\cdot\boldsymbol{r})U_{kn}(r)$, where k is the wavevector.

The matrix elements of the secular equation in a plane-wave basis may be written as follows:

$$\langle k_1|\hat{H}|k_2\rangle = \tfrac{1}{2}k_i^2\delta_{k_1k_2} + \sum_\alpha S^\alpha(q)V_i^\alpha(k_1,k_2) + \frac{4\pi}{|q|^2}\rho(q) + \int \mathrm{d}r\,\mathrm{e}^{\mathrm{i}q\cdot r}\mu_{\mathrm{xc}}(\rho) \qquad (3)$$

where $k_1 = k + G_i$, $k_2 = k + G_j$, $q = G_i - G_j$, $S^\alpha(q)$ is the structure factor for the αth atomic species and G_m are the reciprocal lattice vectors. The contributions of the Coulomb potential can be calculated exactly after Fourier transformation, and those of the exchange–correlation potential are estimated by numerical integration in real space.

Among the interpolation formulae available for the exchange–correlation potential, the two expressions were used in these calculations that have been parametrized later by Perdew and Zunger (1981); i.e. the Ceperley–Alder formula for $r_s > 1$ and Gell-Mann–Brueckner formula of higher accuracy within the limit of high density, leading to

$$\mu_{\mathrm{xc}} = \begin{cases} -\dfrac{0.6193}{r_s} - \dfrac{0.1432}{1+1.0529r_s^{1/2}+0.3334r_s} \\ \quad\times\left(1+\dfrac{0.5264r_s^{1/2}+0.3334r_s}{3(1+1.0529r_s^{1/2}+0.3334r_s)}\right) & r_s > 1 \qquad (4) \\ -0.6193/r_s + 0.031\ln(r_s) - 0.0583 & r_s < 1 \qquad (5) \end{cases}$$

where $r_s = [3/(4\pi\rho)]^{1/3}$ and the first term corresponds to the standard Gaspar–Kohn–Sham exchange potential.

The ionic potential is represented by the norm-conserving non-local pseudopotential of Bachelet *et al* (1982) (BHS). The ionic potential $V_i(r)$ is a j-averaged potential and it allows one to take into account the degeneracies of the $l \pm \frac{1}{2}$ states. The total potential $V_i(r)$ is defined as a sum of the Coulomb potential $V_{\text{core}}(r)$ independent of the orbital quantum number l and the non-local part $\Delta V_l^{\text{ion}}(r)$ formed by the valence electrons:

$$V_i(r) = V_{\text{core}}(r) + \sum_l \Delta V_l^{\text{ion}}(r)\hat{P}_l \tag{6}$$

where $\hat{P}_l$ is a projection operator for the angular momentum l.

The analytical expressions for the second term of equation (3) take the form

$$\langle k+q|V_{\text{core}}(r)|k\rangle = -\frac{4\pi Z_v e^2}{\Omega' q^2}\sum_{i=1}^{2} C_i^{\text{core}} \exp\left(-\frac{q^2}{4\alpha_i^{\text{core}}}\right) \tag{7}$$

$$\langle k_1|\Delta V_l(r)|k_2\rangle = \frac{4\pi}{\Omega'}(2l+1)P_l(\cos\theta_{k_1k_2})T_l \tag{8}$$

where

$$\cos\theta_{k_1k_2} = k_1 \cdot k_2/k_1k_2. \tag{9}$$

Equation (8) goes with the expressions given below for the first four angular momenta:

$$T_0 = \frac{1}{4k_1k_2}\sum_{i=1}^{3}\left(\frac{\pi}{\alpha_i}\right)^{1/2}\left\{\left[A_i + \frac{A_{i+3}}{2\alpha_i}\left(1 - \frac{(k_1-k_2)^2}{2\alpha_i}\right)\right]\exp\left(-\frac{(k_1-k_2)^2}{4\alpha_i}\right) - \left[A_i + \frac{A_{i+3}}{2\alpha_i}\left(1 - \frac{(k_1+k_2)^2}{2\alpha_i}\right)\right]\exp\left(-\frac{(k_1+k_2)^2}{4\alpha_i}\right)\right\} \tag{10}$$

$$T_1 = \frac{1}{4k_1k_2}\sum_{i=1}^{3}\left(\frac{\pi}{\alpha_i}\right)^{1/2}\left\{\left[A_i\left(1 - \frac{2\alpha_i}{k_1k_2}\right) + A_{i+3}\left(\frac{1}{2\alpha_i} + \frac{1}{k_1k_2} + \frac{(k_1-k_2)^2}{2\alpha_i} \times \left(\frac{1}{k_1k_2} - \frac{1}{2\alpha_i}\right)\right)\right]\exp\left(-\frac{(k_1-k_2)^2}{4\alpha_i}\right) + \left[A_i\left(1 + \frac{2\alpha_i}{k_1k_2}\right) + A_{i+3}\left(\frac{1}{2\alpha_i} - \frac{1}{k_1k_2} - \frac{(k_1+k_2)^2}{2\alpha_i}\left(\frac{1}{k_1k_2} + \frac{1}{2\alpha_i}\right)\right)\right]\exp\left(-\frac{(k_1+k_2)^2}{4\alpha_i}\right)\right\} \tag{11}$$

$$T_2 = \frac{1}{4k_1k_2}\sum_{i=1}^{3}\left(\frac{\pi}{\alpha_i}\right)^{1/2}\left\{\left[A_i\left(\frac{12\alpha_i^2}{k_1^2k_2^2} - \frac{6\alpha_i}{k_1k_2} + 1\right) + A_{i+3}\left(\frac{1}{2\alpha_i} + \frac{3}{k_1k_2} - \frac{18\alpha_i}{k_1^2k_2^2} - \frac{3(k_1-k_2)^2}{k_1^2k_2^2} - \frac{(k_1-k_2)^2}{4\alpha_i^2} + \frac{3(k_1-k_2)^2}{2\alpha_i k_1k_2}\right)\right] \times \exp\left(-\frac{(k_1-k_2)^2}{4\alpha_i}\right) + \left[A_i\left(-\frac{12\alpha_i^2}{k_1^2k_2^2} - \frac{6\alpha_i}{k_1k_2} - 1\right)\right.$$

$$+ A_{i+3}\left(-\frac{1}{2\alpha_i}+\frac{3}{k_1k_2}+\frac{18\alpha_i}{k_1^2k_2^2}+\frac{3(k_1+k_2)^2}{k_1^2k_2^2}+\frac{(k_1+k_2)^2}{4\alpha_i^2}\right.$$
$$\left.+\frac{3(k_1+k_2)^2}{2\alpha_ik_1k_2}\right)\Big]\exp\left(-\frac{(k_1+k_2)^2}{4\alpha_i}\right)\Big\} \tag{12}$$

$$T_3=\frac{1}{4k_1k_2}\sum_{i=1}^{3}\left(\frac{\pi}{\alpha_i}\right)^{1/2}\Big\{\Big[A_i\left(1-\frac{12\alpha_i}{k_1k_2}+\frac{60\alpha_i^2}{k_1^2k_2^2}-\frac{120\alpha_i^3}{k_1^3k_2^3}\right)$$
$$+\frac{A_{i+3}}{\alpha_i}\left(\frac{1}{2}+\frac{6\alpha_i}{k_1k_2}-\frac{90\alpha_i^2}{k_1^2k_2^2}+\frac{300\alpha_i^3}{k_1^3k_2^3}-\frac{(k_1-k_2)^2}{4\alpha_i}+\frac{3(k_1-k_2)^2}{k_1k_2}\right.$$
$$\left.-\frac{15\alpha_i(k_1-k_2)^2}{k_1^2k_2^2}+\frac{30\alpha_i^2(k_1-k_2)^2}{k_1^3k_2^3}\right)\Big]\exp\left(-\frac{(k_1-k_2)^2}{4\alpha_i}\right)$$
$$+\Big[A_i\left(1+\frac{12\alpha_i}{k_1k_2}+\frac{60\alpha_i^2}{k_1^2k_2^2}+\frac{120\alpha_i^3}{k_1^3k_2^3}\right)+\frac{A_{i+3}}{\alpha_i}\left(\frac{1}{2}-\frac{6\alpha_i}{k_1k_2}-\frac{90\alpha_i^2}{k_1^2k_2^2}-\frac{300\alpha_i^3}{k_1^3k_2^3}\right.$$
$$\left.-\frac{(k_1+k_2)^2}{4\alpha_i}-\frac{3(k_1+k_2)^2}{k_1k_2}-\frac{15\alpha_i(k_1+k_2)^2}{k_1^2k_2^2}-\frac{30\alpha_i^2(k_1+k_2)^2}{k_1^3k_2^3}\right)\Big]$$
$$\times\exp\left(-\frac{(k_1+k_2)^2}{4\alpha_i}\right)\Big\}. \tag{13}$$

The coefficients A_i^l and exponents α_i are obtained from the BHS article mentioned above. The theoretical framework and main approximations used in these calculations are widely presented in other works as well (see e.g. Bachelet *et al* 1982, Van Camp *et al* 1988, Kolinko 1992, Dovgii *et al* 1991a, b).

The method of special points (Chadi and Cohen 1973) meets the requirements of precise calculation of valence charge density. The secular matrix was diagonalized at special k_i^s-points introduced for the D_{2h} point group by Gashimzade *et al* (1991). Taking into account the non-local character of the calculations, the number of special points has been increased to $M = 16$ and the weighting factors γ_i have been changed correspondingly.

For the immediate $\rho(r)$ calculations, the following expression was used:

$$\rho(r)=\frac{2e}{\Omega|G_0|^2}\sum_{i=1}^{M}\gamma_i\sum_{n=1}^{N_{vz}}\left|\sum_{G_m}a_n(G_m,k_i^s)\sum_{R\in G_0}\exp[-iRG_m\cdot(r-\tau_R)]\right|^2 \tag{14}$$

where the total number of filled bands is $N_{vz}=0.5\sum_\alpha Z_\alpha N_\alpha$.

Self-consistency was achieved by a direct iteration process. In order to accelerate the convergence, ρ_{out}^m was relaxed by means of mixing with 70% output ρ of the $(m-1)$ iteration before their substitution into (4) and (5). The 'starting' Hamiltonian has been constructed in the Thomas–Fermi approximation, which allows mistakes to be avoided in the electronic charge distribution. The self-consistent criterion in the charge-density formalism requires that $|\rho_{out}^m-\rho_{in}^m|<\varepsilon$ after the m_sth iteration step. In the present work, agreement in $E(k)$ eigenvalues within 0.05% between 'input' and 'output' iterations has been adopted as an additional self-consistency criterion. As a result of this, the eigenvalues were stable within the limit 0.01 eV. To get eigenvalues of the Hermitian matrix for 345 plane waves, the *QR* method was used.

In order to establish an accurate description of the electronic density of states, the Hamiltonian has been diagonalized at 16 equally spaced points in 1/8th of the Brillouin zone.

The tetrahedral integration method (Lehman and Taut 1972) was used in these calculations. The same k-point grid was used to evaluate the imaginary part of dielectric function $\varepsilon_2(E)$. Unfortunately, in these calculations a constant matrix element has been used because of the computer's external memory limitation. In doing so, the obtained $\varepsilon_2(E)$ distribution corresponds to the joint density of states (JDOS).

The effective masses of electrons and holes, which are important parameters in discussion of transport properties and exciton effects, are defined by

$$m^*(k_0) = \left. \frac{\hbar^2}{\partial^2 E(k)/\partial k^2} \right|_{k_0} \tag{15}$$

for a k direction about some k_0-point in the Brillouin zone. Band energy values necessary for $m^*(k_0)$ determination at a sequence of points around k_0 have been evaluated immediately (without the scope of kp-perturbation theory).

3. Experimental procedure

InI single crystals were grown from the melt in a sealed quartz ampoule by the Bridgman method. For thorough purification of synthesized materials from traces of bivalent metal impurity and admixtures containing oxygen, the method of vacuum distillation was used. The investigation of oxygen (1s) and carbon (1s) core levels showed that their admixtures remained negligibly small in the process of measurement. That is why the obtained samples of InI single crystals can be considered qualitative enough and free from contaminants.

X-ray photoelectron analysis has been performed in high-vacuum conditions ($\simeq 10^{-9}$ Torr), since InI is sensitive to humidity. An Al Kα monochromatized beam of radiation (with photon energy $h\nu = 1486.6$ eV) was focused on the surface of the sample. An electron gun of low energy was used for charge compensation during spectra registration. The energy of emitted electrons was determined by means of a semi-spherical analyser and spectrometer (Perkin–Elmer), and the signal obtained has been registered by an HP9836C spectral analyser.

4. Results and discussion

The lattice parameters of InI single crystals are as follows (Jones and Templeton 1955): $a = 0.475$ nm, $b = 1.276$ nm, $c = 0.491$ nm. As is shown in figure 1, this is a layered structure, and the cell contains four molecular units, whereas the primitive cell contains only two of them. The unit cell presented in the figure possesses three adjacent layers perpendicular to the b axis. Each In^+ cation is surrounded by seven nearest-neighbour anions. Furthermore, such a structure can be considered as intermediate between those of NaCl (coordination 6) and CsCl (coordination 8); the layer containing AB (or CD) atoms resembles the distorted NaCl lattice, while the layer with BC atoms leads to a CsCl-like lattice. The reciprocal lattice vectors are as follows: $B_1 = (2\pi/a, 2\pi/b, 0)$, $B_2 = (-2\pi/a, 2\pi/b, 0)$, $B_3 = (0, 0, 2\pi/c)$. The atomic sites in the primitive cell are determined by the following vectors: $\tau_{1,\mathrm{In}} = (0, -0.398, -0.25)$, $\tau_{1,\mathrm{I}} = (0, -0.145, -0.25)$, $\tau_{2,\mathrm{In}} = (0, 0.398, 0.25)$, $\tau_{2,\mathrm{I}} = (0, 0.145, 0.25)$; and all four atoms possess the same C_s local symmetry. On this evidence InI single crystals are optically biaxial with the optical axes along the three

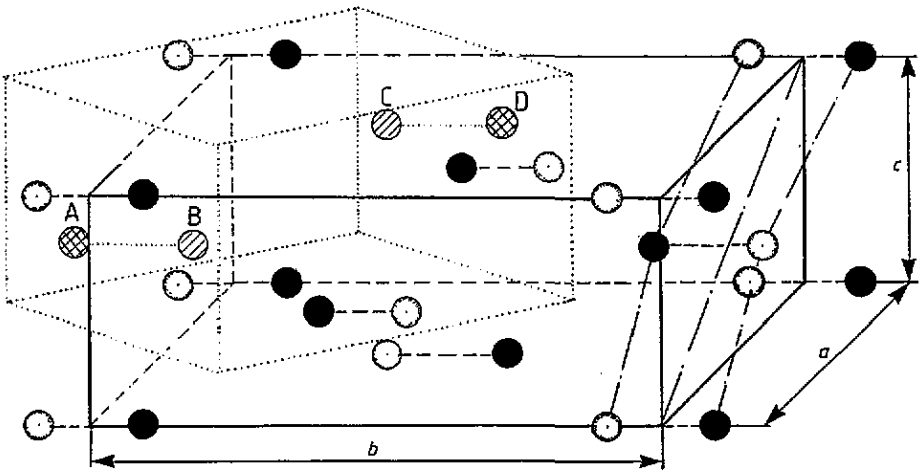

Figure 1. Crystal structure of indium iodide together with lattice parameters a, b and c. Filled circles represent indium ions and open circles iodine ions. The primitive cell is labelled by dotted lines and the corrugated surface of layered packets is shown by chain lines.

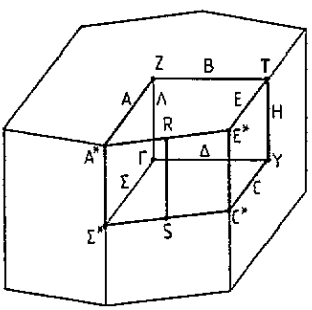

Figure 2. Brillouin zone of the face-centred orthorhombic lattice. The points of symmetry (with the exception of Σ^*, C^*, A^*, E^* and B) are labelled according to Kovalev (1965).

crystallographic axes. For a full description of the crystal structure, the reader is referred to the article of Jones and Templeton (1955).

To obtain the zone diagram $E(k)$ after self-consistent potential determination, the energies have been tabulated at 259 points, localized at edges and lines of high symmetry in the irreducible part of the Brillouin zone (see figure 2).

The band structure for indium iodide (see figure 3) is displayed along high-symmetry lines in the hexagonal Brillouin zone. A self-consistent band diagram has been obtained after 14 cycles of the self-consistent iteration process. With two molecular units in the primitive cell of InI, 10 occupied valence bands have been obtained. Table 1 presents a list of all the relevant energy eigenvalues at the symmetry points of the Brillouin zone. In table 2 the allowed dipole transitions at the T, Z, S, Y and Γ points and on the Δ, Σ, H and Λ lines in D_{2h}^{17} space group are summarized; the D_{2h} point group is the minor group of the k-vector for the Γ and Y points and the minor group is C_{2v} point group for all the remaining points and lines presented in figure 2. From table 1 it is seen that the smallest interband intervals of the forbidden gap are formed far from the Γ point. This typical location peculiarity of gaps at the edge of the Brillouin zone arises immediately from the electronic configuration of the 10-electron compounds with their surplus s-electron pair. The calculated valence band possesses rather negligible dispersion in k-space, except for the lines directed towards

Table 1. Energy-band eigenvalues (eV) of indium iodide at high-symmetry and some other points of common type of the Brillouin zone as obtained in the present calculation.

Γ (0, 0, 0)		Y (0, 1, 0)		Σ* (0.56, 0, 0)		S (0.5, 0.5, 0)		H* (0, 1, 0.344)	
$\Gamma^+_{1,v}$	−11.7	$Y^+_{1,v}$	−11.4	$\Sigma^*_{1,v}$	−11.1	$S^+_{1,v}$	−11.1	$H^*_{1,v}$	−11.2
$\Gamma^-_{3,v}$	−10.7	$Y^-_{3,v}$	−11.0	$\Sigma^*_{4,v}$	−10.8	$S^-_{2,v}$	−10.7	$H^*_{3,v}$	−10.9
$\Gamma^+_{1,v}$	−3.98	$Y^+_{1,v}$	−4.87	$\Sigma^*_{1,v}$	−5.48	$S^+_{1,v}$	−5.39	$H^*_{1,v}$	−5.24
$\Gamma^-_{3,v}$	−3.41	$Y^-_{3,v}$	−3.29	$\Sigma^*_{4,v}$	−4.32	$S^-_{2,v}$	−4.48	$H^*_{3,v}$	−4.72
$\Gamma^+_{1,v}$	−3.17	$Y^+_{4,v}$	−2.92	$\Sigma^*_{1,v}$	−2.85	$S^+_{1,v}$	−2.60	$H^*_{2,v}$	−2.54
$\Gamma^+_{2,v}$	−3.07	$Y^+_{2,v}$	−2.75	$\Sigma^*_{2,v}$	−2.32	$S^+_{2,v}$	−2.38	$H^*_{3,v}$	−2.20
$\Gamma^+_{4,v}$	−2.62	$Y^-_{4,v}$	−2.45	$\Sigma^*_{3,v}$	−2.23	$S^+_{1,v}$	−2.32	$H^*_{1,v}$	−2.05
$\Gamma^-_{2,v}$	−2.33	$Y^-_{2,v}$	−1.99	$\Sigma^*_{4,v}$	−2.06	$S^-_{1,v}$	−2.14	$H^*_{4,v}$	−2.02
$\Gamma^-_{4,v}$	−2.03	$Y^+_{1,v}$	−1.03	$\Sigma^*_{1,v}$	−0.79	$S^-_{2,v}$	−0.74	$H^*_{1,v}$	−0.80
$\Gamma^-_{3,v}$	−0.92	$Y^-_{3,v}$	−0.86	$\Sigma^*_{4,v}$	0	$S^-_{2,v}$	−0.16	$H^*_{3,v}$	−0.03
$\Gamma^+_{2,c}$	3.72	$Y^+_{1,c}$	1.82	$\Sigma^*_{2,c}$	1.88	$S^+_{2,c}$	1.92	$H^*_{3,c}$	1.83
$\Gamma^+_{1,c}$	3.96	$Y^+_{2,c}$	3.23	$\Sigma^*_{1,c}$	2.49	$S^+_{1,c}$	2.46	$H^*_{1,c}$	2.40
$\Gamma^-_{2,c}$	3.97	$Y^-_{3,c}$	4.38	$\Sigma^*_{1,c}$	2.54	$S^-_{2,c}$	2.72	$H^*_{2,c}$	3.43
$\Gamma^-_{3,c}$	4.41	$Y^-_{2,c}$	4.61	$\Sigma^*_{1,c}$	3.10	$S^+_{1,c}$	3.25	$H^*_{4,c}$	3.70
$\Gamma^+_{4,c}$	5.25	$Y^-_{3,c}$	4.80	$\Sigma^*_{3,c}$	3.80	$S^-_{1,c}$	3.61	$H^*_{1,c}$	4.28
$\Gamma^-_{4,c}$	5.32	$Y^+_{4,c}$	4.90	$\Sigma^*_{4,c}$	5.80	$S^-_{2,c}$	5.31	$H^*_{3,c}$	4.65
$\Gamma^-_{3,c}$	6.00	$Y^-_{4,c}$	6.11	$\Sigma^*_{1,c}$	7.19	$S^-_{2,c}$	7.53	$H^*_{1,c}$	6.94

Table 2. Allowed dipole transitions in the case of the space group D^{17}_{2h} ($CmCm$).

Point	$E\|\|a$	$E\|\|b$	$E\|\|c$	Line	$E\|\|a$	$E\|\|b$	$E\|\|c$
Γ(Y)	$\Gamma^+_1\Gamma^-_2$	$\Gamma^+_1\Gamma^-_3$	$\Gamma^+_1\Gamma^-_4$	Δ	$\Delta_1\Delta_4$	$\Delta_1\Delta_1$	$\Delta_1\Delta_3$
	$\Gamma^+_2\Gamma^-_1$	$\Gamma^+_2\Gamma^-_4$	$\Gamma^+_2\Gamma^-_3$		$\Delta_2\Delta_3$	$\Delta_2\Delta_2$	$\Delta_2\Delta_4$
	$\Gamma^+_3\Gamma^-_4$	$\Gamma^+_3\Gamma^-_1$	$\Gamma^+_3\Gamma^-_2$		$\Delta_3\Delta_2$	$\Delta_3\Delta_3$	$\Delta_3\Delta_1$
	$\Gamma^+_4\Gamma^-_3$	$\Gamma^+_4\Gamma^-_2$	$\Gamma^+_4\Gamma^-_1$		$\Delta_4\Delta_1$	$\Delta_4\Delta_4$	$\Delta_4\Delta_2$
	$\Gamma^-_1\Gamma^+_2$	$\Gamma^-_1\Gamma^+_3$	$\Gamma^-_1\Gamma^+_4$				
	$\Gamma^-_2\Gamma^+_1$	$\Gamma^-_2\Gamma^+_4$	$\Gamma^-_2\Gamma^+_3$	Σ	$\Sigma_1\Sigma_1$	$\Sigma_1\Sigma_4$	$\Sigma_1\Sigma_3$
	$\Gamma^-_3\Gamma^+_4$	$\Gamma^-_3\Gamma^+_1$	$\Gamma^-_3\Gamma^+_2$		$\Sigma_2\Sigma_2$	$\Sigma_2\Sigma_3$	$\Sigma_2\Sigma_4$
	$\Gamma^-_4\Gamma^+_3$	$\Gamma^-_4\Gamma^+_2$	$\Gamma^-_4\Gamma^+_1$		$\Sigma_3\Sigma_3$	$\Sigma_3\Sigma_2$	$\Sigma_3\Sigma_1$
					$\Sigma_4\Sigma_4$	$\Sigma_4\Sigma_1$	$\Sigma_4\Sigma_2$
Z(T)	Z_1Z_2	Z_1Z_1	Z_1Z_1				
	Z_2Z_1	Z_2Z_2	Z_2Z_2	H(Λ)	H_1H_4	H_1H_3	H_1H_1
					H_2H_3	H_2H_4	H_2H_2
S	$S^+_1S^-_2$	$S^+_1S^-_2$	$S^+_1S^-_1$		H_3H_2	H_3H_1	H_3H_3
	$S^-_1S^+_2$	$S^-_1S^+_2$	$S^-_1S^+_1$		H_4H_1	H_4H_2	H_4H_4
	$S^+_2S^-_1$	$S^+_2S^-_1$	$S^+_2S^-_2$				
	$S^-_2S^+_1$	$S^-_2S^+_1$	$S^-_2S^+_2$				

the centre of the Brillouin zone. The smallest direct gap is located at the H line and its value corresponds to 1.86 eV ($H_{3,v} \rightarrow H_{3,c}$). Although usually band gaps are seriously underestimated in the local-density approximation, in this case for InI there turns out to be good agreement with experiment. For comparison, the experimental value is 2.0229 eV (Jin *et al* 1989). In spite of the fact that the agreement between the calculated gap and experiment can be improved by treating the exchange coefficient, this approach will be avoided here. However, the peak of the valence band is localized at the Σ* point (0 eV) on the Σ line when the minimum of the conduction band is localized at the Y point (1.82 eV). In such a way the indirect gap is 0.04 eV smaller than the direct gap, which draws a final conclusion about

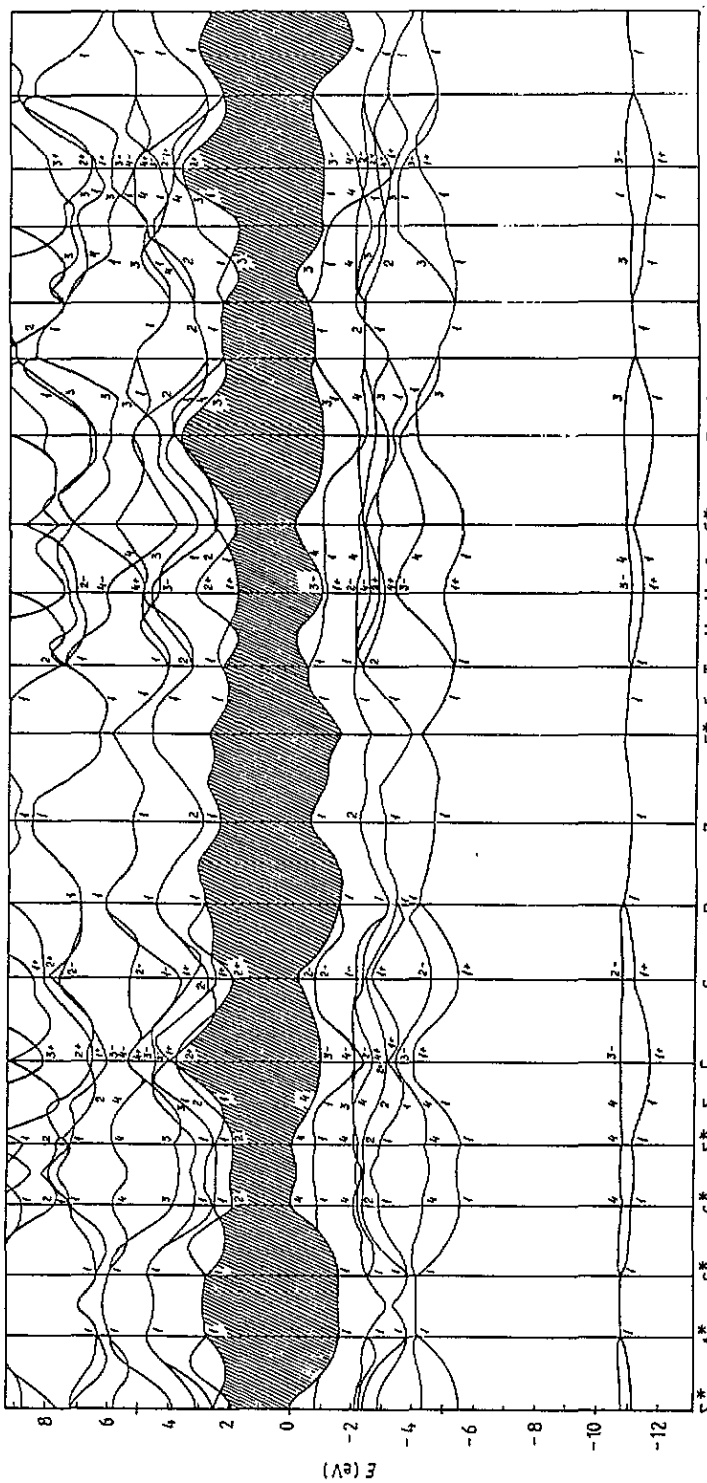

Figure 3. Valence and lower conduction bands of InI. Energies are measured from the top of the valence band.

the character and localization places of transitions that are responsible for fundamental absorption edge formation. Besides, attention should be paid to the presence of optima whose energy values are too close to one another against the peak of the valence complex (e.g. $S_2^- = -0.16$ eV) and those against the conduction band minimum ($\Sigma_{2,c}^* = 1.88$ eV; $S_{2,c}^+ = 1.92$ eV and the whole line segment [C*;Σ*]). It should be noted that inspection of the charge density of the highest occupied band and also the lowest conduction band suggests a reason for the relatively weak sensitivity of the forbidden gap to the scaling of the exchange potential. As the $\Gamma_{2,c}^+$–$\Sigma_{2,c}^*$ states are bonding states with a density localized along cation–cation directions, they would possess a weak response towards enhancement of the exchange potential. On the other hand, the $\Gamma_{1,c}^+$ valence band is a delocalized I $5p_y$ state (cation In p orbitals predominate at the Σ* point) and is consequently indifferent to the exchange scaling. In Bloch-sum representations the $\Gamma_1^+(Y_1^+)$ state is described as $(1/\sqrt{2})(s^1 + s^2) + (1/\sqrt{2})(p_y^1 - p_y^2) + (1/\sqrt{2})(d_{x^2-y^2}^1 + d_{x^2-y^2}^2) + (1/\sqrt{2})(d_{3z^2-r^2}^1 + d_{3z^2-r^2}^2)$, where the upper index corresponds to the atom number (kind of atom does not matter because the local symmetry of all atoms is the same). The following Bloch expansions can be obtained for Σ_1 and $\Gamma_2^+(Y_2^+)$ states by omitting the constant multiplier and d terms (for the reason that d electrons are 'frozen' in the core): $(s^1 + s^2) + (p_x^1 + p_x^2) + (p_y^1 - p_y^2)$ and $(p_z^1 - p_z^2)$, respectively. But then $\Gamma_{3,v}^-$–$\Sigma_{4,v}$ states are antibonding states having a density that is perceptibly localized near the atomic sites; they are sensitive to the variation of the exchange–correlation potential. As Γ_1^-, Γ_3^+, Y_1^- and Y_3^+ irreducible representations are not connected with s and p states, their absence in figure 3 is justified.

For the $T_{1,v} \rightarrow T_{1,c}$ direct transition a value of 2.67 eV was obtained. This transition is forbidden only for $\boldsymbol{E}\|\boldsymbol{a}$ in the case of the simple group, whilst the smallest transitions ($H_{3,v} \rightarrow H_{3,c}$; $\Sigma_{4,v}^* \rightarrow \Sigma_{2,c}^*$, 1.88 eV; $S_{2,v}^- \rightarrow S_{2,c}^+$, 2.08 eV) are forbidden for two polarizations ($\boldsymbol{E}\|\boldsymbol{a}$ and $\boldsymbol{E}\|\boldsymbol{b}$). Because of the mechanical properties of InI crystals, optical measurements up to now have been performed only in the ac plane, which is why a comparison of the band–band transition distribution with reflection spectra for $\boldsymbol{E}\|\boldsymbol{b}$ polarization would be especially interesting. Besides, low $E(k)$ dispersion at Brillouin zone boundaries makes possible low-energy optical transitions at other points (especially at points of common type). In this case rigorous account of relativistic effects can change the consecutive order of interband transition values. Still the group-theoretical analysis demonstrates that spin–orbit interaction does not introduce additional splitting of levels at the Γ, Y, Z, T, S and Σ points. For the T point, for example, the resolution of the binary group states into states of simple group $T_i \times D^{(1/2)}$ (where $D^{(1/2)}$ are the representations of the rotation group) gives the result (T_1,T_2:T_5,T_6). In such a way, taking into account spin–orbit interactions, levels become doubly degenerate (at least at high-symmetry points and at ones on the Brillouin zone edges, which is of primary importance) and the selection rules for allowed dipole transitions will be reduced. For precise definition of localization points of the smallest transitions in the Brillouin zone, $E(k)$ calculations for other isostructural indium halides (InBr, InCl) would be useful. It should be noted that the calculated band-gap data can be defined more exactly by extending the theory beyond the limits of the local-density approximation.

The results of calculations of hole and electron effective masses at the valence band maxima and the conduction band minima demonstrate considerable anisotropy. After suitable averaging of the direction-dependent masses over a number of angles, the average value of hole mass m_h^* at the Σ* valence band maximum comes to 0.177 (hereafter values quoted are in units of free-electron mass). However, in the Brillouin zone centre direction (Γ point) and the S point the calculated m_h^* values are 0.522 and 0.594 respectively, whereas the effective mass parallel to the z axis is estimated as 0.118. For the following maximum

at the H line (−0.028 eV) the average value of the hole effective mass is 0.296. Though experimental values of hole effective masses that can be determined, e.g. using cyclotron resonances or transport measurements, are absent, it would be expected that the calculated values would be somewhat undervalued because they do not take into account important effects for such types of layered compounds, i.e. those caused by electron–phonon interaction and polarons. Values of electron effective masses were determined at two points: at the Y point (1.82 eV), which is connected with the indirect gap according to the results obtained, and at the point of minimum direct gap on the H line (1.83 eV). For the point on the H line the calculated value m_e^* comes to 0.247. For the Y point two effective masses have been evaluated: m_{eL}^* along the C line equal to 2.538, and transverse m_{eT}^* equal to 0.215. The calculated total density-of-states mass is $m_d^* = (6^2 m_{eL}^* m_{eT}^{*2})^{1/3} = 1.616$. These estimations possess forecasting character too, since experimental values that can be obtained from electroreflectance measurements or from cyclotron resonance have not yet been published.

As mentioned earlier, the determination of localization places and the ordering of the lowest interband intervals of orthorhombic In and Tl monohalides are the subject of some controversy. The analysis of partial contributions to the electron density of orthorhombic TlI (Kolinko *et al* 1992a) showed that the lowest conduction bands are formed by metal p_z orbitals. Besides, the $\rho(r)$ distribution amongst the atoms of adjacent layers resembles a π-like bond (for the $\Gamma_{2,c}^+$ state only the contribution is mentioned up to I $5p_z$ orbitals). The top of the valence band is formed by cation 5s orbitals and halogen $5p_y$ orbitals. These characteristic features of charge distribution in the region of the forbidden gap are observed for InI as well. In such a way optical absorption in the case of orthorhombic $A^{III}B^{VII}$ halides is mainly induced by intra-cation transition. On the other hand, the experimental investigations (Yoshida *et al* 1984) on solid solutions of mixed isostructural $InBr_{1-x}I_x$ crystals demonstrate that the lowest-energy peak in reflection spectra is formed from the transition on the metal sublattice, since no significant changes occur in consequence of the change in halogen concentration. Therefore the $E(k)$ electron spectra of TlI and InI should be supposed to differ essentially in the region of bands forming the forbidden gap. This supposition was actually confirmed by the calculation given: in the TlI case the fundamental absorption edge is topologically defined at the T point and on the S line, whilst the lowest InI transitions, as is seen from figure 3 and table 1, originate from the other points. It is necessary to note that in the case of TlI in both calculations (Van Dyke and Samara 1975, Kolinko *et al* 1992a) the band energy values have not been tabulated along the Σ line.

For more profound understanding of the optical and mechanical anisotropy of indium iodide, data on electron charge density are necessary, because knowledge of its distribution gives useful information about the chemical bond. Figure 4 demonstrates contour plots of the charge-density distribution for valence electrons in the different planes. They were calculated according to formula (14) by summing over all valence bands (n index) and sampling 16 special k_i^s-points in the irreducible Brillouin zone. It should be noted that the cross section in the ac plane (see figure 4(c)) intersects the centres of halogen atoms. That is why, taking into account the corrugated surface of layered packets, it becomes evident that the contour plot of cation atoms is not a cross section through their centres. Figures 4(a) and (b) incorporate two formula units, which refer to adjacent layers. One can see that in the case of InI the electrons are transferred from around the cation to the anion, and the covalent character coexists with the ionic one. Other characteristic features obtained from the present study are summarized as follows: (i) extra charge appears along the ⟨0 1 0⟩ directions at points about 0.155 nm away from the centre of each In and I atom; (ii) charge distributions show (figure 4(c)) rather weak deviations from the spherical distribution towards second-nearest neighbours; and (iii) the excess charge

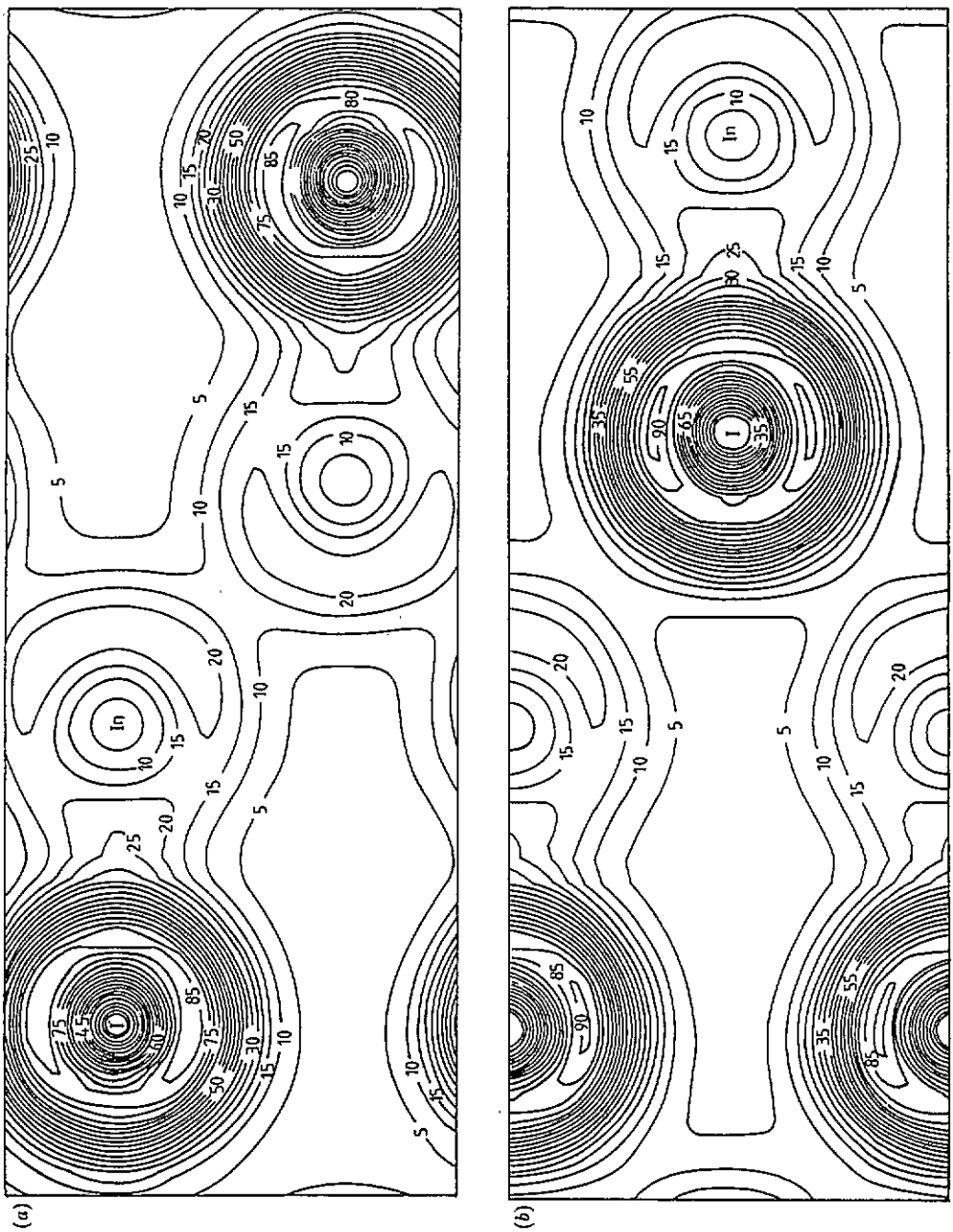

Figure 4. Outlines of the total charge-density distribution of InI in the different planes: (*a*) *bc* plane; (*b*) *ab* plane; (*c*) *ac* plane. Results are given in electrons/cell (normalized to unity).

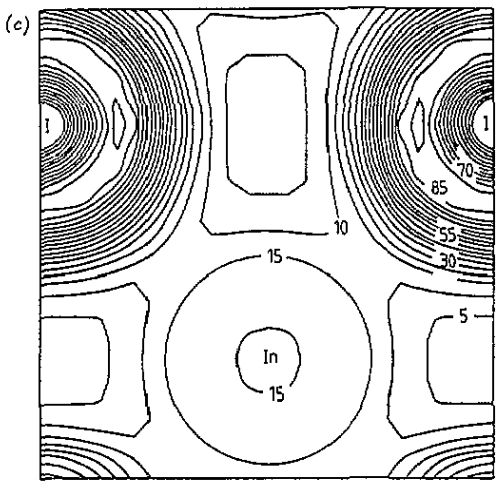

Figure 4. (Continued)

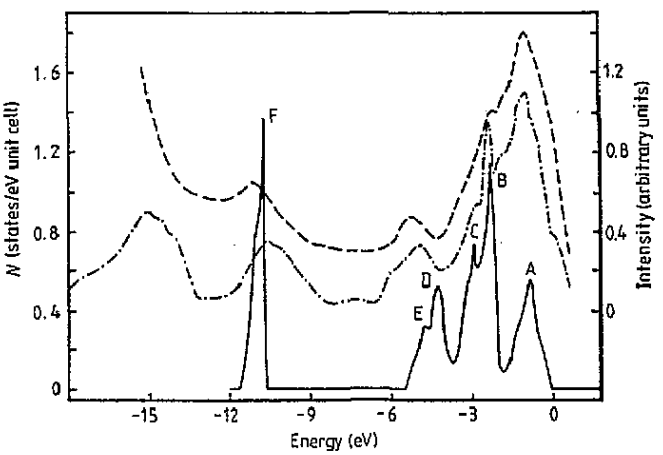

Figure 5. Calculated density of states for indium iodide (full curve). X-ray photoemission data (broken curve, Porte (1982); chain curve, results obtained in this work) are superimposed. The peaks labelled by A, B, C, D, E and F are discussed in the text.

accumulates in the region between neighbouring atoms of indium. The last point refers to an intermolecular bond, since the third-nearest neighbours of each In ion are the two In ions lying in the next layer; they are slightly more distant (at 3.5%) than the second-nearest neighbours. Figures 4(*a*) and (*b*) demonstrate the existence of cation–cation hybridization and the absence of anion orbital mixing. At the same time, the significant ionic background does not allow one to reveal the presence of a saddle point and to determine the genetic origin of the intermolecular cation–cation bonding in the *bc* plane. Analysis of total charge density and partial contributions of the different irreducible representations shows that In s orbitals remain fully occupied; in contrast the In p orbitals play a more passive role in the valence region formation. Unfortunately, at present, data on nuclear magnetic resonance

experiments for InI are absent, but the results for TlI (Novoselov *et al* 1970, 1971) are consistent with non-negligible covalent contributions to two phases (D_{2h}^{17} and O_h^1).

Table 3. Peculiarities of electronic density of states. The energies are in eV and the valence band maximum is referenced to zero.

Feature	Experiment	Theory
A	−1.0	−0.90
B	−2.4	−2.23
C	−2.9	−2.92
D	−4.9	−4.32
E	−5.4	−4.76
F	−10.5	−10.75

One of the most widely used experimental probes of semiconductor ground-state eigenvalues is photoelectron spectroscopy. The calculated density of states (DOS) for InI is presented and compared to the experimental results of x-ray photoemission spectroscopy (XPS) in figure 5. The XPS results obtained by Porte (1982) are reproduced in the same figure. Also, the features observed in the calculated and experimental spectra are listed in table 3. The XPS measurements determine the full valence band width equal to 11.8 eV, which can be compared with the calculated value of 11.66 eV (according to Porte the experimental value is somewhat higher and amounts to 12.1 eV).

In figure 6 the partial contributions of the different energetically separated subbands to the total valence charge density are shown. On the basis of charge-density analysis the density of states should be divided into three general regions: iodine (5p)–indium (5s, 5p) states, indium (5s)–iodine (5p) bonding states and iodine (5s) core-like states. Here, one can start with the lower-lying (~ -12 eV) valence bands in figure 3. These bands (which are singly and doubly degenerate according to the symmetry of the D_{2h}^{17} structure), as illustrated in figures 6(*a*) and (*b*), are derived primarily from the s-type orbitals located at two different iodine atoms, but at the Y and Γ points there exists a very small admixture of p orbitals. In the middle part of the occupied band region, the peak D and the weak shoulder E at ~ -6 eV (in Porte's (1982) results the shoulder was not resolved) do not line up with the two peaks of I p_x–In s states of the third and fourth bands (see figure 3) and the relative shift makes up approximately 1 eV. In spite of the fact that combination of these states varies with k-wavevector, they can practically be identified as bonding orbitals between indium and halogen atoms (see figures 6(*c*) and (*d*)). The D peak is determined by the feature at the Σ^* point, where $\Sigma_{4,v}^*$ (-4.32 eV) is a bonding combination of indium s orbitals and iodine p orbitals, which resembles a σ_{s-p}-like intramolecular bond. The shoulder E is topologically identified also with doubly degenerate states in the region of the Z point. The bonding combination of the same I p–In s orbitals oriented along the I–In–In–I chain and forming a cation–cation intermolecular bond causes the feature E.

The top part of the valence band, from the valence band maximum (which is referenced to zero level as a datum) to approximately -3.8 eV, is predominantly composed on In s and iodine p-like orbitals as illustrated in figures 6(*e*) and (*f*). This region demonstrates three maxima (labelled in figure 5 by A, B and C), also indicated by experiment. These maxima have been examined via density maps of valence electrons. While peak A is determined by states on the Y–Γ line that include the cation s states as well, the two other peaks (B, C) correspond mainly to halogen p orbitals. The uppermost peak B determined by the states at the Σ^* point and on the T–Z segment is of a more 'non-bonding' nature than the other two

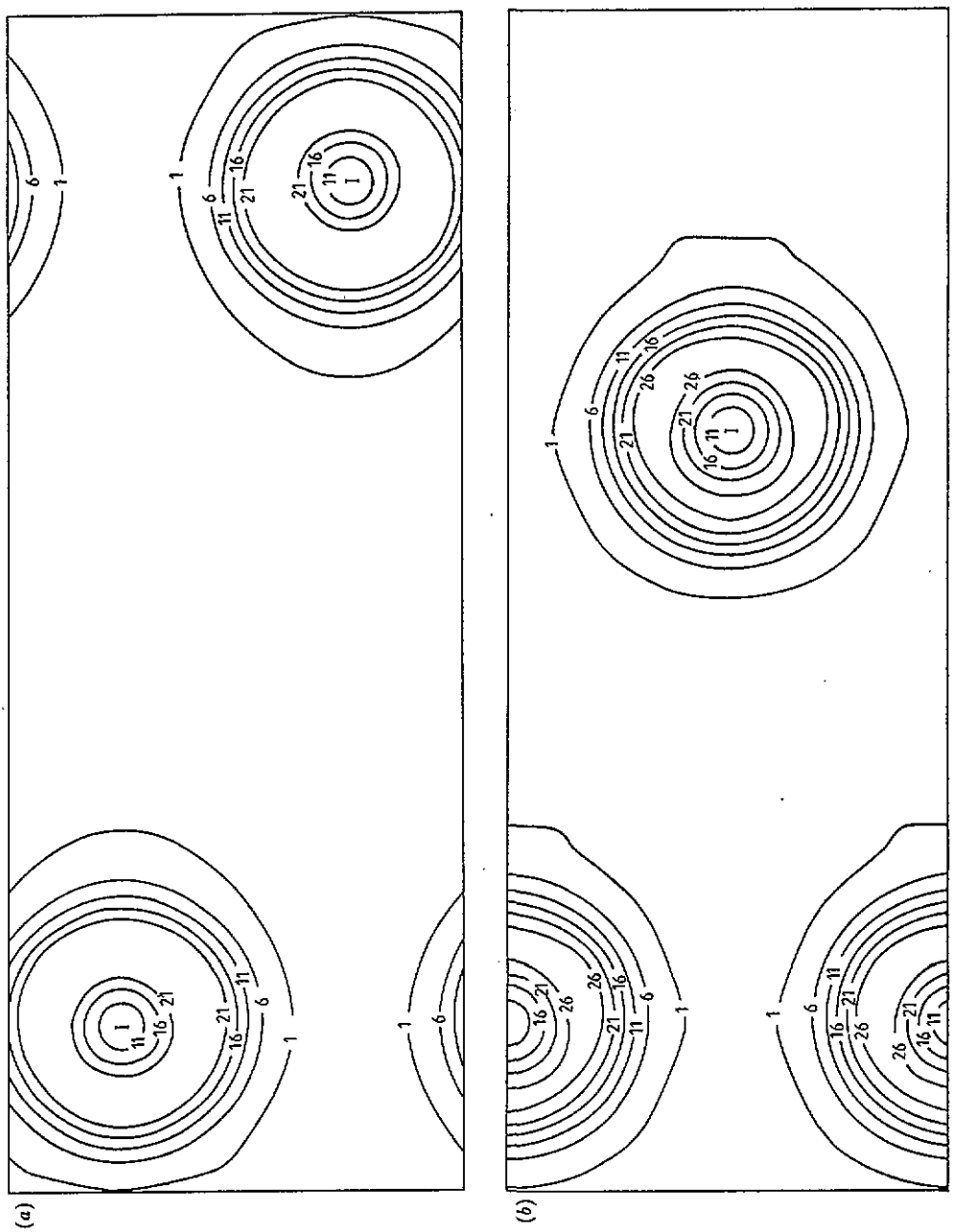

Figure 6. Valence charge-density contour plots of the different energetically separated subbands for the electronic density-of-states features in indium iodide: partial contribution of the bands in the energy regions $-12 < E < -10.5$ eV (a, b), $-5.5 < E < -3.8$ eV (c, d) and $-3.8 < E < 0$ eV (e, f). The charge densities are plotted in the bc (a, c, e) and ab planes (b, d, f).

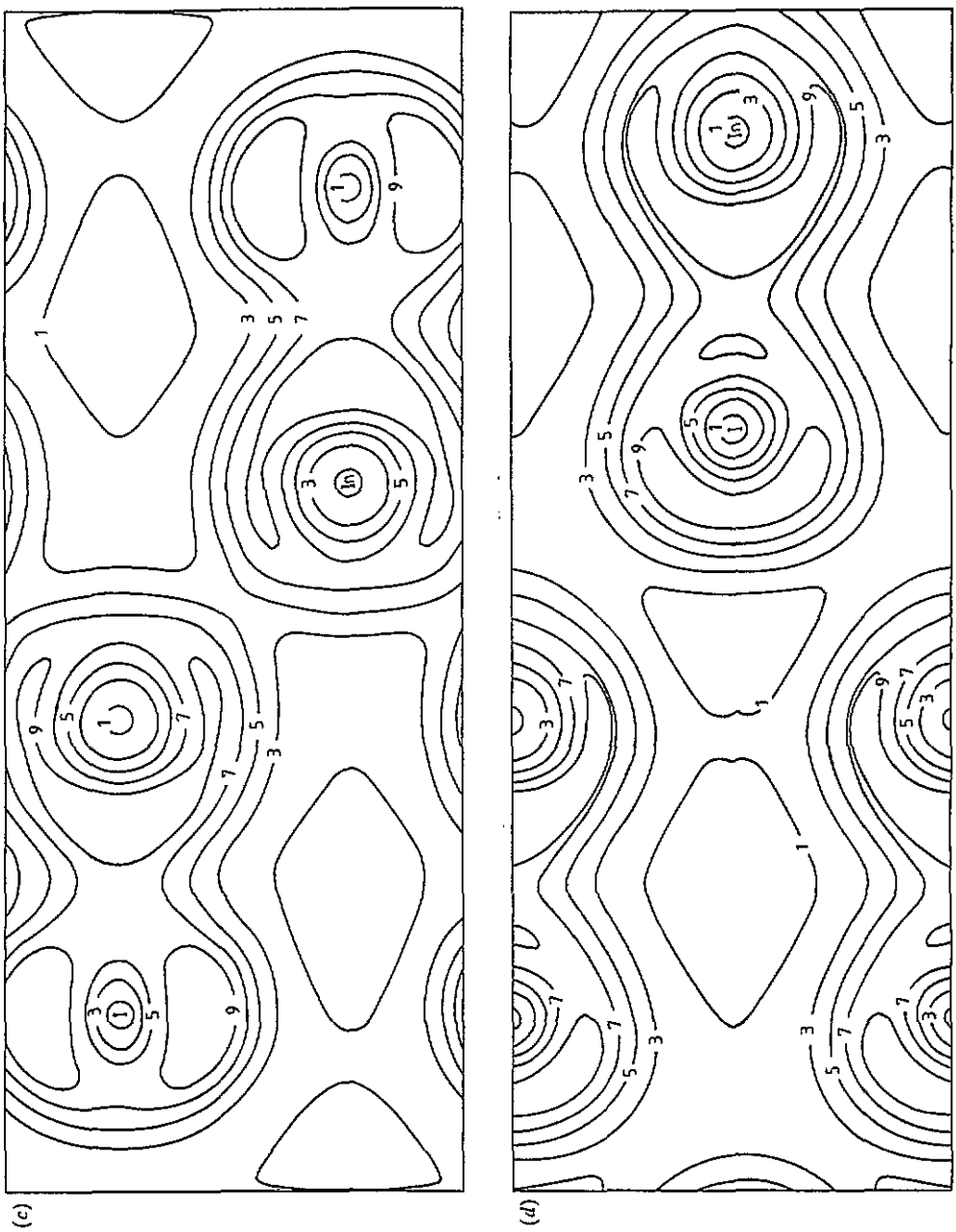

Figure 6. (Continued)

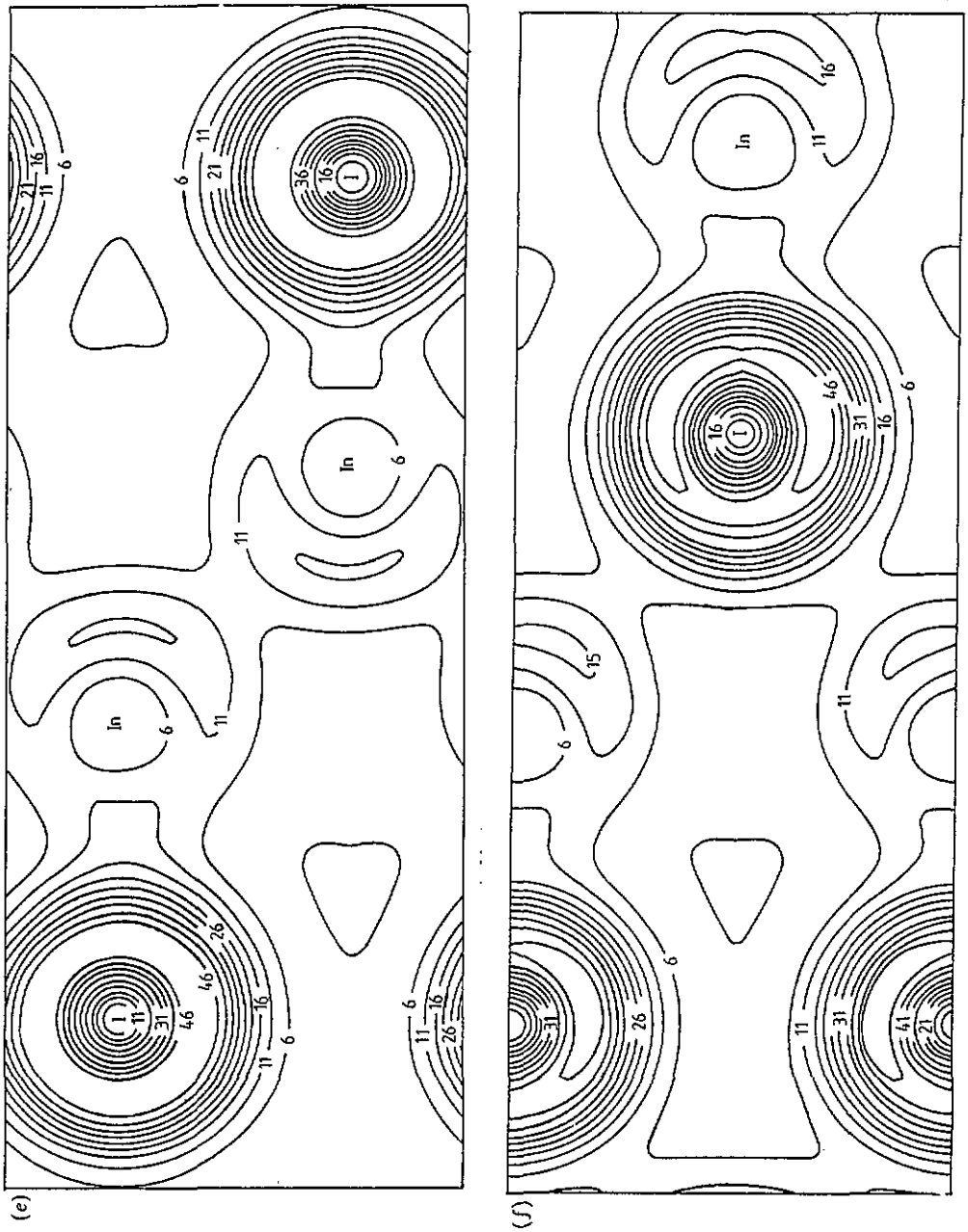

Figure 6. (Continued)

(A, C). In the case of $B_{2,v}(T_{2,v}–Z_{2,v})$ and $\Sigma_{3,v}$ states, p_x- and p_z-like orbitals are localized on the iodine and are not oriented along the bonding directions. Because of the small overlap among these orbitals (especially along S and B lines), the bands are almost dispersionless. Although the fine structure of the upper portion of the valence band is not fully resolved in the experimental spectra, the general agreement is good. It should be noted that results of DOS calculation reproduce the experimental spectra both in the deep energy regions and in the region near E_F. Theoretical–experimental agreement in the case of low-lying localized orbitals (peak F in figure 5) is somewhat unusual. It would be interesting to check up the conformity of deeper-lying orbital location (i.e. in figure 5 it can be seen that both photoemission spectra in the -17 eV region contain the band that corresponds to indium d states). The largest effect would have been expected if the outermost core orbitals, namely the In 4d and I 4d, had been excluded from the frozen core and had been included in the variational procedure. Owing to limited computer resources, however, it was impossible to perform this variation in a self-consistent way.

Finally, in figure 7 are presented the calculated results for the imaginary part of the $\varepsilon_2(E)$ dielectric constant of indium iodide single crystals performed using the constant matrix element. Because of the absence of an experimental plot for $\varepsilon_2(E)$, one should be restricted to stating that comparison with reflection spectra obtained by Nakamura *et al* (1987) at 0–10 eV gives a good display of the main optical spectra structures. Measurements of the InI optical spectra for different light polarizations and the corresponding ε_2 calculations by the Kramers–Kronig method are in progress. A detailed analysis will be the subject of a forthcoming publication.

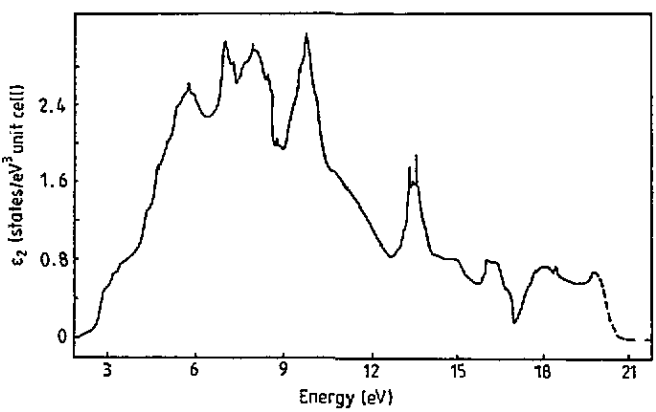

Figure 7. The imaginary part of the dielectric constant, as computed with the constant matrix element for direct transitions in indium iodide with the band structure of the present paper.

5. Summary and conclusions

For the study of the properties of the $A^{III}B^{VII}$ family, for the first time the electronic structure of InI single crystals has been investigated by means of self-consistent pseudopotentials within the local-density approximation. The end results for indium iodide have revealed that the state distributions of InI and orthorhombic TlI have similar features, but there exists a distinction in the determination of localization places and the ordering of the lowest

interband intervals. Ground-state properties as well as optical data have been calculated and shown to be in good agreement with experiments, thus confirming the validity of the assumed approach and the accuracy of the results obtained. No adjustable parameters based upon experimental data entered the calculation. Calculations for the band structure, electronic density of states, hole and electron effective masses, optical response functions and charge density are presented. The main features of the calculated band structure are the following: the band gap is 1.82 eV and is found to be indirect ($\Sigma^*_{4v} \rightarrow Y^+_{1,c}$); the smallest direct interval is located on the H line and its value corresponds to 1.86 eV, which is 0.04 eV larger than those of the indirect gap; the two lowest core-like bands are formed exclusively by halogen s electrons; the following two bands are shaped mainly from In s and I p orbitals; the higher valence bands and the lower conduction bands originate mainly from the I p, In s states and the In p_z, I p_z states, respectively; the lowest optical transitions were calculated as cationic in character and are dominated by In 5s→In $5p_z$ transitions. The resulting band structure showed good agreement with the measured forbidden gap (~ 2.0 eV), as well as with photoemission (within ~ 0.3 eV) data, which can now be unambiguously interpreted. Thus it can be concluded that this treatment describes realistically the one-particle properties of indium iodide.

References

Bachelet G, Hamann D R and Schlüter M 1982 *Phys. Rev.* B **26** 4199

Blonskii I V, Krochuk A S, Stetsishin T L and Franiv A V 1986 *Sov. Phys.–Solid State* **28** 1764

Blonskii I V, Lun' Yu O, Franiv A V and Bigun M V 1992 *Ukr. Fiz. Zh.* **37** 547

Brodin M S, Blonskii I V, Bigun M I, Lun' Yu O and Franiv A V 1992 *Ukr. Fiz. Zh.* **37** 977

Chadi D J and Cohen M L 1973 *Phys. Rev.* B **8** 5744

Clayman B P, Nemanich R J, Mikkelsen J C and Lucovsky G 1982 *Phys. Rev.* B **26** 2011

Dovgii Ya O, Kityk I V, Kolinko M I, Krochuk A S, Franiv A V and Zamorskii M K 1991a *Sov. Phys.–Solid State* **33** 225

—— 1991b *Phys. Status Solidi* b **167** 637

Dovgii Ya O, Krochuk A S and Kolinko M I 1990 *Preprint* Inst. Theor. Phys., Acad. Sci. USSR (Kiev) No 23 (in Russian)

Gashimzade F M, Gusejnova D A and Aliev A M 1989 *Sov. Phys.–Solid State* **31** 21

Hamann D R, Schlüter M and Chiang C 1979 *Phys. Rev. Lett.* **43** 1494

Hohenberg P and Kohn W 1964 *Phys. Rev.* B **136** 864

Jin F, Itoh T and Goto T 1989 *J. Phys. Soc. Japan* **58** 2586

Jones R E and Templeton D H 1955 *Acta Crystallogr.* **8** 847

Kityk I V, Kolinko M I and Franiv A V 1992 *Ferroelectrics* **130** 347

Kobayashi K 1976 *Festkörperprobleme (Advances in Solid State Physics 16)* ed J Treusch (Braunschweig: Vieweg) p 117

Kohn W and Sham L J 1965 *Phys. Rev.* A **140** 1133

Kolinko M I 1992 *Ukr. Fiz. Zh.* **37** 117

Kolinko M I, Kityk I V and Krochuk A S 1992a *J. Phys. Chem. Solids* **53** 1315

Kolinko M I, Krotschuk A S and Kityk I V 1992b *Phys. Status Solidi* a **134** K93

Kovalev O V 1965 *Irreducible Representations of the Space Groups* (New York: Gordon and Breach) p 234

Krochuk A S, Kityk I V, Kolinko M I and Franiv A V 1991 *Zh. Prykl. Spectrosk.* **55** 142

Lehman G and Taut M 1972 *Phys. Status Solidi* **54** 469

Levy F and Mooser E 1972 *Helv. Phys. Acta* **3** 69

Lowdes P P and Perry C H 1978 *J. Chem. Phys.* **58** 271

Nakamura K, Sasaki Y, Watanabe M and Fujita M 1987 *Phys. Scr.* **35** 557

Novoselov S K, Baidakov L A and Strakhov L P 1970 *Sov. Phys.–Solid State* **12** 915

—— 1971 *Vestnik Leningrad Univ. Ser. Him.–Fiz. Nauk* **10** 54

Ohno N, Fujita M, Nakai Y and Nakamura K 1978 *Solid State Commun.* **28** 137

Ohno N, Nakamura K and Nakai Y 1986 *J. Phys. Soc. Japan* **55** 3659

Ohno N, Nakamura K and Nakai Y 1987 *J. Phys. Soc. Japan* **56** 2565

Ohno N, Yoshida M, Nakamura K and Nakai Y 1980 *Solid State Commun.* **35** 775
—— 1985 *Solid State Commun.* **53** 569
Otto P, Wagner F and Beck H P 1992 *Phys. Rev.* B **45** 2654
Perdew J and Zunger A 1981 *Phys. Rev.* B **23** 5048
Porte L 1982 *Solid State Commun.* **42** 85
Porte L and Maire J-C 1980 *Solid State Commun.* **33** 481
Van Camp P E, Van Doren V E and Devreese J T 1988 *Phys. Status Solidi* b **146** 573
Van Dyke J P and Samara G A 1975 *Phys. Rev.* B **11** 4935
Yoshida M, Ohno N, Watanabe H, Nakamura K and Nakai Y 1984 *J. Phys. Soc. Japan* **53** 408